$X\ ^1\Sigma^+$ and $a\ ^3\Sigma^+$ states of LiCs studied by Fourier-transform spectroscopy

Peter Staanum,[1,*] Asen Pashov,[2] Horst Knöckel,[1] and Eberhard Tiemann[1]
[1]*Institut für Quantenoptik, Gottfried Wilhelm Leibniz Universität Hannover, Welfengarten 1, 30167 Hannover, Germany*
[2]*Department of Physics, Sofia University, 5 James Bourchier Boulevard, 1164 Sofia, Bulgaria*
(Received 1 December 2006; published 26 April 2007)

We present the first high-resolution spectroscopic study of LiCs. LiCs is formed in a heat-pipe oven and studied via laser-induced fluorescence Fourier-transform spectroscopy. By exciting molecules through the $X\ ^1\Sigma^+$-$B\ ^1\Pi$ and $X\ ^1\Sigma^+$-$D\ ^1\Pi$ transitions vibrational levels of the $X\ ^1\Sigma^+$ ground state have been observed up to 3 cm^{-1} below the dissociation limit enabling an accurate construction of the potential. Furthermore, rovibrational levels in the $a\ ^3\Sigma^+$ triplet ground state have been observed via singlet-triplet mixing in the higher excited states. With the help of coupled channels calculations, accurate singlet and triplet ground-state potentials were derived reaching the atomic ground-state asymptote. These potentials yield an accurate determination of the singlet and triplet ground-state dissociation energies and allow first predictions of cold collision properties of Li+Cs pairs.

DOI: 10.1103/PhysRevA.75.042513 PACS number(s): 31.50.Bc, 33.20.Kf, 33.20.Vq, 33.50.Dq

I. INTRODUCTION

Spectroscopy of heteronuclear diatomic alkali-metal molecules provides important input to current research in cold molecules and mixtures of ultracold atomic gases. Cold heteronuclear alkali-metal dimers is a subject of great interest since they can be formed at temperatures below 1 mK [1–5] and possess a significant permanent electric dipole moment for deeply bound singlet levels [6,7]. Based on this combination of properties, feasible proposals for electric field control of ultracold collisions [8,9] and cold chemical reactions [10,11] were set forward. Furthermore, cold heteronuclear alkali-metal dimers are promising candidates for applications in quantum computation [12]. Precise potential energy curves, in particular for the lowest electronic states, are evidently important for such applications as well as for understanding the molecule formation processes (photoassociation), rovibrational state selective detection [5,13] and for formation of vibrational ground-state molecules [14]. In ultracold mixtures of atomic gases, quantum degeneracy of one atomic species can be achieved through sympathetic cooling by the other species [15–17]. The interspecies interaction strength can be varied through magnetic Feshbach resonances and has a large influence on a variety of effects such as phase-separation between a Bose-Einstein condensate and a degenerate Fermi gas [18] and the transition to a Bardeen-Cooper-Schrieffer superfluid state in dilute Fermi gases [19]. Understanding interspecies collision properties at the atomic ground-state asymptotes requires precise potential curves of the electronic ground states, for example for predicting the magnetic field strength values of Feshbach resonances at zero kinetic energy.

Cold LiCs molecules were observed very recently, being formed in a two-species magneto-optical trap [1]. Previously, inelastic collisions [20] and sympathetic cooling of Li by Cs in an optical dipole trap [21] have been studied. Recent theoretical work considers LiCs in strong dc electric fields and its influence on rovibrational dynamics [22] and Li-Cs collision cross sections [9].

Although LiCs was observed already in 1928 by Walter and Barratt through absorption in a mixture of metallic vapors [23], very few spectroscopic studies, none of them at high resolution, have been made until now. In the early 1970s Kanes *et al.* [24] determined parameters for the LiCs singlet ground state potential from measurements of the velocity dependence of the Li($2s$)+Cs($6s$) collision cross section. In the 1980s Vadla *et al.* studied the repulsive Li($2p$)+Cs($6s$) asymptote [25]. More recently LiCs molecules were formed on He nanodroplets and excitation spectra of the $d\ ^3\Pi \leftarrow a\ ^3\Sigma^+$ transition were recorded and modeled [26]. *Ab initio* potentials were calculated by Korek *et al.* [27] (see Fig. 1) and more recently an extended theoretical study was made by Aymar and Dulieu [6]. These theoretical potentials provide a good starting point for analysis of the spectra obtained in the present work.

Here we present a high-resolution spectroscopic study of the LiCs molecule. Similar to our previous studies [28,29] we apply Fourier-transform spectroscopy of laser-induced fluorescence from LiCs molecules formed in a heat pipe, because this technique is suitable for collecting a large amount of accurate experimental data. By using properly chosen excitation schemes (see e.g. [28,29]) we can measure transition frequencies to a wide range of vibrational levels in the singlet $X\ ^1\Sigma^+$ as well as in the triplet $a\ ^3\Sigma^+$ ground states, especially levels close to the asymptote. Since the two states are coupled at long internuclear distances by the hyperfine interaction it is not correct to treat them separately in this region, as to do so would lead to model potentials which are unable to reproduce the experimental observations close to the asymptote. Therefore, the aim of our experimental work is to collect experimental data on both ground states and to find accurate experimental potential energy curves simultaneously for both states—the indispensable starting point for a study of the molecular structure of LiCs or for modeling of cold collision processes on the Li($2s$)+Cs($6s$) asymptote. The potential curves directly yield an accurate determination of important quantities such as dissociation energy and equilibrium internuclear distance. Furthermore, we apply these

*Present address: Institute of Physics and Astronomy, University of Aarhus, Denmark.

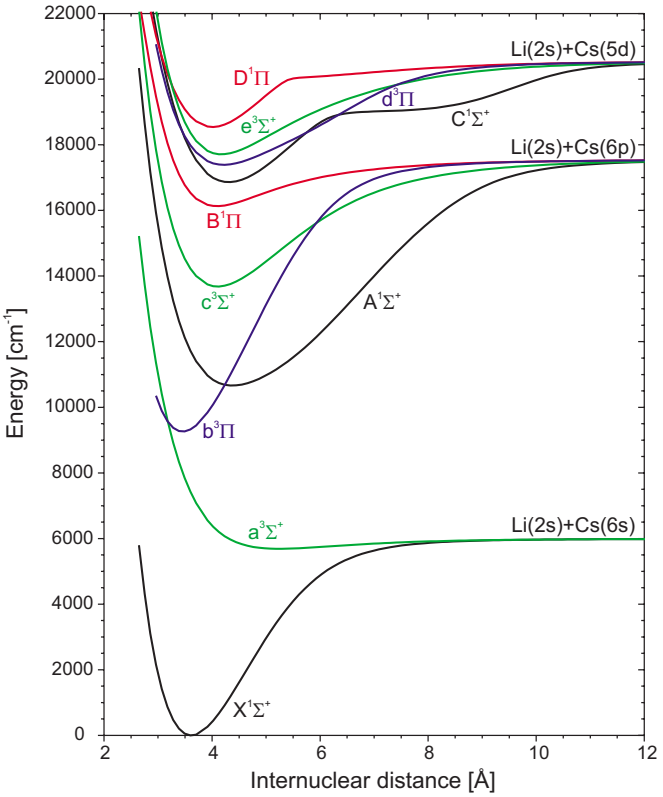

FIG. 1. (Color online) Selected singlet and triplet potential energy curves in LiCs [27].

potential curves within a coupled channels model in order to explain our experimental observations and also to compute collision properties for comparing recent results of sympathetic cooling of Li by Cs [21].

This paper is organized as follows: The experimental setup and excitation schemes are presented in Sec. II. In Sec. III we describe the analysis of the obtained spectra. The procedure for construction of potential energy curves is described in Sec. IV and the potentials are reported. In Sec. V we apply our potentials to cold collision studies and in Sec. VI we give our conclusion and an outlook for further experimental study needed for a quantitative description of ultracold collisions in Li+Cs.

II. EXPERIMENT: MOLECULE FORMATION AND SPECTROSCOPY

A. Molecule formation

LiCs molecules are formed in a stainless steel heat pipe identical to the one described in Ref. [30], except for one modification described below. The heat pipe (960 mm long and 34 mm outer diameter) is filled with 6 g Li and 5 g Cs (the Cs, in a closed ampoule, is loaded into the side container [30,45,44]) and typically operated with 3–6 mbar Ar buffer gas pressure.

Since the vapor pressure difference between Li and Cs at a common temperature is extremely large, we modified the design of Ref. [30] in order to obtain a three-section heat pipe, which is more suitable for producing a vapor mixture with similar concentrations of Li and Cs and hence for forming LiCs molecules [31]. In Ref. [30] the central 60 cm of the heat pipe is heated uniformly in a commercial oven (Carbolite); here we mount two stainless steel shells (20 cm long, 50 mm inner diameter) concentrically around the heat pipe and seal up the ends facing towards the center of the oven such that only the central 20 cm of the heat pipe are heated directly in the oven. By blowing air into the open ends, which extend outside of the oven, we can maintain a lower temperature in the sections shielded by the shells than in the central part of the heat pipe.

The heat pipe is conditioned by heating it to temperatures of about 580 °C under 10 mbar Ar pressure; subsequently the Cs ampoule is broken by shaking the tube. Operating temperatures are 540 °C in the central part and 370 °C in the outer sections. The heat-pipe oven was operated for more than 200 hours over a 10 month period and was still in good working condition at the end of this period.

B. Laser-induced fluorescence Fourier-transform spectroscopy

Laser-induced fluorescence from LiCs molecules is observed after excitation on the $B\,^1\Pi \leftarrow X\,^1\Sigma^+$ and $D\,^1\Pi \leftarrow X\,^1\Sigma^+$ transitions. The $B\,^1\Pi \leftarrow X\,^1\Sigma^+$ transitions were excited using a Coherent 599 dye laser (with DCM dye) at frequencies in the range 15 529–16 032 cm^{-1} and a Coherent 699 dye laser at frequencies in the range 16 397–17 022 cm^{-1} (with rhodamine 6G dye as well as with a mixture of rhodamine 6G and rhodamine B). The $D\,^1\Pi \leftarrow X\,^1\Sigma^+$ transition was excited using the dye laser with rhodamine 6G at frequencies in the range 16 663–17 239 cm^{-1} and a frequency doubled Nd:YAG laser. The strongest signals were observed for the $B\,^1\Pi \leftarrow X\,^1\Sigma^+$ system and we studied the ground states mainly through this system. Indeed, we note that Walter and Barratt observed strong absorption in the range 15 983–16 582 cm^{-1} [23] which according to Fig. 1 corresponds to the $B\,^1\Pi \leftarrow X\,^1\Sigma^+$ transition. At excitation frequencies in the range ~14 900–15 400 cm^{-1}, we find strong fluorescence due to Li_2 and NaCs (Na is present as an impurity in the Li sample) which overshadows a possible LiCs signal. Using an Ar-ion laser for excitation at 457.9 nm, 476.5 nm, 488.0 nm, 496.5 nm, and 514.5 nm we did not observe any fluorescence from LiCs molecules, only from Li_2, LiNa, and NaCs.

Contrary to the previously studied molecules NaRb [28] and NaCs [29], the low-lying levels of the excited $B\,^1\Pi$ state in LiCs turned out to be almost free of local perturbations by the neighboring triplet states $b\,^3\Pi$ and $c\,^3\Sigma^+$, which could be expected from the theoretical potential curves (see Fig. 1). As a consequence we were unable to register any transition to the triplet ground state from the low lying $B\,^1\Pi$ state levels. We searched instead for access to the triplet manifold through local perturbations in the $D\,^1\Pi$ and $C\,^1\Sigma^+$ states. Here we used a coumarine 6 dye laser with a typical power of 25 mW. Unfortunately within the searched excitation frequency region of 18 446–19 039 cm^{-1} we were also not able to register transitions to the triplet ground state.

The only fluorescence to the $a\,^3\Sigma^+$ state is observed after excitation to high-lying levels in the $B\,^1\Pi$ state. The transi-

tions are due not to local perturbations by individual rovibrational levels of nearby triplet states [28,29], but rather to homogeneous singlet-triplet configuration mixing at large internuclear separations, which eventually leads to angular momentum recoupling into Hund's case (c). This conclusion is supported first by the observation that high-lying B state levels seem to be locally unperturbed. Second the intensity distribution of progressions from the high-lying B state levels to the ground singlet state can be explained satisfactorily by the Franck-Condon factors between the X and the B states, including the highest v_X'' levels (contrary to the case of NaRb [28]). This means that transitions from these B state levels to high-lying $a\,^3\Sigma^+$ state levels will become probable when the B state changes its character from Hund's case (a) $^1\Pi$ to Hund's case (c) $\Omega=1$ at long internuclear distances. Indeed, in our spectra we find transitions mainly to high v_a'' and none to the bottom of the triplet ground state.

The laser-induced fluorescence light is collected in the direction opposite to the one of laser beam propagation and recorded by a Bruker IFS 120HR Fourier-transform spectrometer (FTS). For detection we use a photomultiplier (Hamamatsu R928) or a Si-photodiode. In order to avoid illumination of the detector by the He-Ne laser (632.8 nm), used in the FTS for calibration and stepping control, a notch filter (8 nm full width at half-maximum) is introduced in the beam path. This also suppresses the fluorescence induced in the corresponding spectral region. The resolution of the FTS is typically set to $0.03-0.05\ \mathrm{cm}^{-1}$. The uncertainty of the line positions is estimated to be 1/10 of the resolution. For lines with signal-to-noise ratio less than 3 the uncertainty is gradually increased. Each spectrum results typically from an average of 10–20 scans, but the number of scans is varied from 5 to 350 depending on the signal strength for the features of interest in the spectra. For improving the signal-to-noise ratio, the spectral window for some spectra is limited by using color glass filters or interference filters. In order to facilitate the identification in such cases we recorded also a spectrum at the same excitation frequency without filters, but with lower resolution ($0.1\ \mathrm{cm}^{-1}$) and a smaller number of scans.

A list of all excitation frequencies used in these experiments together with the assignment of the excitation transitions are given in Tables III and IV of the supplementary materials [32].

III. ANALYSIS OF SPECTRA

A. The $X\,^1\Sigma^+$ state

Assignment of the large number of transitions, about 6600, to the $X\,^1\Sigma^+$ state is done in an iterative process; by gradually improving the potential for the $X\,^1\Sigma^+$ state, more and more transitions can be correctly assigned.

Initially, we identify several strong doublet series which are clearly recognized as P-R components from the regular development of the doublet spacing. Among these series we choose those with similar spacing, i.e., with similar rotational quantum numbers. Based on the theoretical potential for the $X\,^1\Sigma^+$ state [27] we make an initial guess for the vibrational and the rotational quantum numbers of these fluorescence progressions. The quantum numbers that give the closest agreement with the theoretical vibrational and rotational spacings are assigned and a small set of Dunham coefficients is fitted. If the fit is successful we can use the fitted coefficients to assign new progressions; if not, a reassignment of the quantum numbers must be made. After some iterations we obtain a self-consistent set of assigned experimental progressions which can be satisfactory described by a few Dunham coefficients. This is a first hint of a correct rotational numbering. Here we point out the very good quality of the theoretical calculations [6,27]; the theoretical rotational numbering needed a correction by only two or three units.

When the list of assigned transitions reaches several hundreds we perform the first potential fits. Initially, we start with a pointwise potential (defined in Sec. IV) based on the theoretical curve [27] and improve it using the procedure described in Ref. [33]. In the further analysis of the spectra we apply this pointwise potential curve, since outside the range of the fitted v'' and J'' it usually possesses better predictive properties than the Dunham-type coefficients. Moreover our experience from previous studies [28,30] shows that a potential curve which fits long vibrational progressions recorded at high precision in a wide range of rotational quantum numbers also indicates the correctness of the vibrational numbering.

Finally, the established vibrational numbering was confirmed by assigning several progressions for the less abundant $^6Li^{133}Cs$ molecule. These progressions fit to the experimental potential based only on $^7Li^{133}Cs$ data when the appropriate reduced mass is applied [34].

In order to describe the important long-range part of the potential, it is of great value to collect data with transitions to high-lying levels of the ground state. Since we noticed during the measurements that transitions to such high-lying levels originate from high-lying vibrational levels of the $B\,^1\Pi$ state, we studied this state in order to optimize the experimental conditions for observation of near asymptotic levels in the $X\,^1\Sigma^+$ state (a report on the $B\,^1\Pi$ state can be found in Ref. [35]). From the available experimental term energies of the $B\,^1\Pi$ state levels a preliminary potential for the $B\,^1\Pi$ state was fitted. This potential was then used to predict transition frequencies for excitation transitions with large Franck-Condon factors. In this way we systematically recorded transitions from $v'=24$ and 25 to the $X\,^1\Sigma^+$ state for a wide range of J', thus adding several rovibrational levels with $v_X''=49$ and 50 to the ground-state data set. In most cases such high-lying levels of the $X\,^1\Sigma^+$ state could be observed with a suitable signal-to-noise ratio only by increasing the number of summed scans to several hundred. We searched for excitations to higher vibrational levels of the $B\,^1\Pi$ state within predicted spectral regions but we were not able to register fluorescence from $v'\geqslant 26$ to the $X\,^1\Sigma^+$ state, probably because of predissociation or unfavorable transition probabilities.

B. The $a\,^3\Sigma^+$ state

The triplet transitions are easily distinguished by their hyperfine structure (HFS), which at our resolution consists of

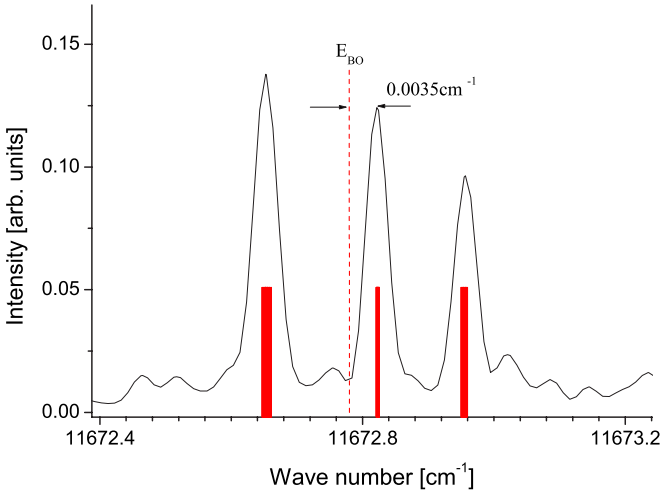

FIG. 2. (Color online) Hyperfine structure of a transition to the $v_a''=9$, $N_a''=17$ level of the $a\ ^3\Sigma^+$ state. The vertical full lines indicate the prediction of the coupled channels calculation. The dashed vertical line indicates the position of the hyperfine-structure free level, which is shifted by 0.035 cm^{-1} from the central component of the structure.

three lines split by approximately 0.3 cm^{-1}. Calculations similar to those in Ref. [36] show that the observed splitting is well reproduced by the Fermi contact interaction model applying the atomic HFS constants for ^{7}Li and ^{133}Cs [37]. In Fig. 2 a transition to the triplet state level $v_a''=9$, $N_a''=17$ [46] is shown together with the prediction of the splitting modeled by a coupled channels calculation as described in Sec. IV. A larger portion of the same progression originating from the $v'=25$, $J'=17$ $B\ ^1\Pi$ state level excited by a Q-type ($\Delta J=0$) transition is shown in Fig. 3. Some of the transitions reach near asymptotic levels in both ground states. The vertical dashed lines indicate the prediction of the coupled channels calculation for $J''=N''=17$ in which the hyperfine interaction between the states is included. The progression to the $X\ ^1\Sigma^+$ state is formed by Q lines whereas the progression to

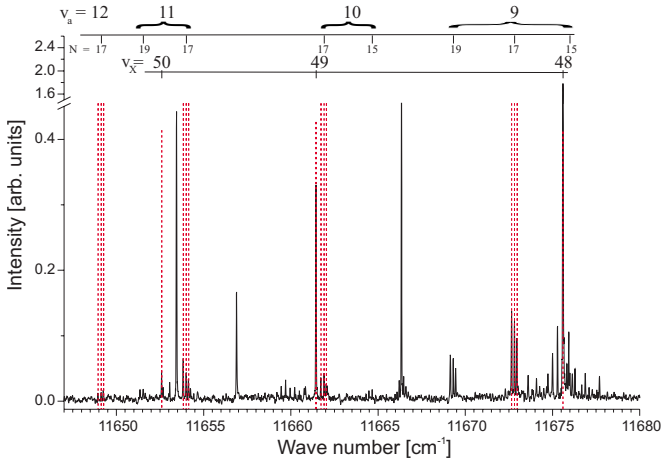

FIG. 3. (Color online) Portion of recorded progression from the B state level with $v'=25$, $J'=17$ excited by a Q-type transition. Lines not marked on the figure belong to another assigned progression.

the $a\ ^3\Sigma^+$ state consists of transitions to $N_a''=15$, 17, and 19. Lines not marked in the figure belong to another progression also assigned and used in our analysis.

The rotational assignment of the triplet lines is straightforward since we always find the progression to the $X\ ^1\Sigma^+$ state that shares the excited level in the $B\ ^1\Pi$ state with the progression to the $a\ ^3\Sigma^+$ state. The vibrational assignment of the transitions to the triplet ground state is done in the same way as for the $X\ ^1\Sigma^+$ state, however, no transitions in ^{6}Li^{133}Cs were observed and hence the vibrational assignment relies only on the internal consistency of the total procedure.

C. Data sets

Altogether about 6600 transitions to the $X\ ^1\Sigma^+$ state (130 of them belong to ^{6}Li^{133}Cs) and 180 transitions to the $a\ ^3\Sigma^+$ state in ^{7}Li^{133}Cs were assigned (see Tables I and II of the supplementary materials [32]). The corresponding distribution of vibrational and rotational quantum numbers is shown in Fig. 4. For the $X\ ^1\Sigma^+$ state we observe transitions to $v_X''=0-50$ in ^{7}Li^{133}Cs. The set of $a\ ^3\Sigma^+$ state vibrational levels covers $v_a''=4-12$ and the vibrational numbering established in this study agrees with that from the theoretical potential. The limited number of experimental data, however, might lead to a revision of this assignment in the future, if additional data on the $a\ ^3\Sigma^+$ state are collected. Although the data set for the $a\ ^3\Sigma^+$ state might seem fragmentary compared to our similar studies in other molecules, the collection of these data is extremely valuable. This is first because of the limited possibilities for exciting triplet states in LiCs, and second since a proper description of the Li($2s$)+Cs($6s$) asymptote is only possible if both the $X\ ^1\Sigma^+$ state and $a\ ^3\Sigma^+$ state are treated in a coupled channels manner as described in the next section.

IV. CONSTRUCTION OF POTENTIAL ENERGY CURVES

The self-consistent assignment and fitting procedure described above gives rise to accurate pointwise short-range potentials [33]. For the long-range (LR) part of both potentials we use an extension of the form

$$U_{\mathrm{LR}}(R) = U_\infty - \frac{C_6}{R^6} - \frac{C_8}{R^8} - \frac{C_{10}}{R^{10}} \pm E_{\mathrm{ex}}. \tag{1}$$

Here U_∞ is the energy of the atomic asymptote with respect to the minimum of the $X\ ^1\Sigma^+$ state potential, C_6, C_8, and C_{10} are the dispersion coefficients and

$$E_{\mathrm{ex}}(R) = A_{\mathrm{ex}} R^\gamma e^{-\beta R} \tag{2}$$

is the frequently applied functional form of the exchange energy [38] that is added for the triplet state and subtracted for the singlet state.

The pointwise short-range and the long-range potentials are connected at a point R_o ensuring a smooth transition between both potential branches. R_o is chosen as described in Refs. [28,39], the C_6 and C_8 coefficients are fixed to their theoretical values [40–42], γ and β are estimated using the ionization potentials for Li and Cs [43] according to Ref.

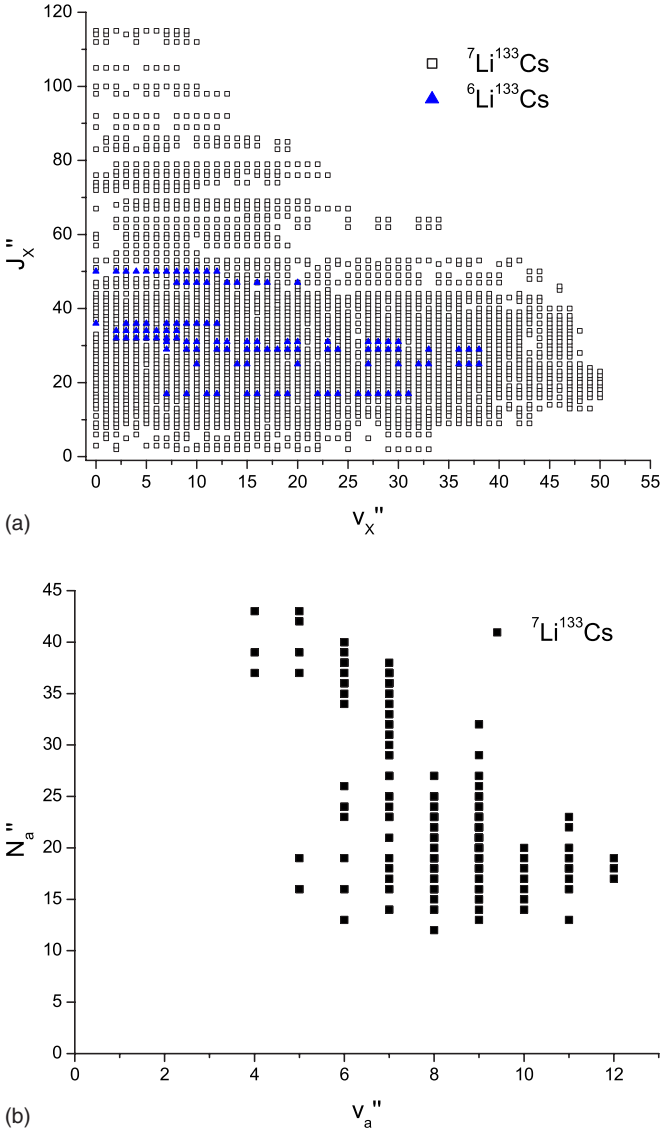

FIG. 4. (Color online) Observed rovibrational levels in the $X\ ^1\Sigma^+$ and $a\ ^3\Sigma^+$ states of $^7Li^{133}Cs$ and $^6Li^{133}Cs$.

[38], while U_∞, C_{10}, and A_{ex} are adjusted during the fitting procedure.

In the first step of the fitting procedure we adjust only the pointwise part of the potential for the $X\ ^1\Sigma^+$ state. The experimental transition frequencies are fitted by adjusting the parameters of the pointwise potential and the term energies of the excited levels.

Since we choose the origin of the potential energy at the minimum of the $X\ ^1\Sigma^+$ state potential, in the second step of the fitting procedure we need to determine the term energies of the $a\ ^3\Sigma^+$ state levels with respect to the $X\ ^1\Sigma^+$ state. We do this using spectra where we observe simultaneously progressions to the singlet and the triplet states originating from a common upper state level. For a given singlet ground-state potential we calculate the term energies of the triplet state using the energy of the excited level, determined in the previous step, and the progression to the $a\ ^3\Sigma^+$ state from this level. These $a\ ^3\Sigma^+$ term energies are then used to fit the potential parameters of the triplet state. In this way we always ensure a proper position of the $a\ ^3\Sigma^+$ state with respect to the $X\ ^1\Sigma^+$ state.

In order to treat the hyperfine structure of the spectral lines of the triplet state we confirmed that in the experimental data the splitting is, within our resolution, independent of the vibrational and rotational quantum numbers v'' and N'' (except for very few cases, which we discuss below). Therefore, we use the central component of the structure for identification of the transition (see Fig. 2). We convert the observed frequency to term energy, and take into account the shift ($-0.035\ cm^{-1}$, which means the hyperfine level is more deeply bound than the unperturbed level) of the selected hyperfine component from the unperturbed, hyperfine structure free one. Thus we fit with the constructed term values a Born-Oppenheimer potential.

For high vibrational levels, and especially in cases of close approach of singlet and triplet levels with the same rotational quantum numbers, significant deviations from the Born-Oppenheimer picture can be expected [28,29]. In $^7Li^{133}Cs$ this is most pronounced for $v_X''=49$ in the singlet and $v_a''=10$ in the triplet state (see Fig. 3). The deviations of the transitions determined by the Born-Oppenheimer potentials [indicated with thick (blue) bars in Fig. 5] from the experimental ones are significant and reach $0.06\ cm^{-1}$ for $v_X''=49$ and $J'=24$. Figure 5 shows the development from low J to high J.

Therefore, in a third step, the Born-Oppenheimer potentials are refined by extending the single channel approach from the first two steps and applying a coupled channels calculation as discussed in detail in Refs. [28,29]. Briefly, we calculate the difference between the single channel and coupled channels eigenvalues and subtract these differences from the experimentally observed transition frequencies in order to obtain the frequencies that would be observed without hyperfine coupling between the singlet and the triplet ground states. Next, these frequencies are used in a combined fit to adjust the parameters of the long-range extensions of the potentials, as well as in separate fits (described for the first two steps) of the short-range pointwise part of the triplet and singlet potentials. Finally, the whole fitting procedure is repeated until the frequencies predicted with the coupled channels calculations agree with the experimental observations. The importance of the coupled channels calculation is illustrated in Fig. 5, where the predictions for the coupled system are shown with thin (red) bars together with the experimentally observed lines and the single channel predictions [thick (blue) bars]. The degree of mixing between the triplet and singlet levels is characterized by the expectation value of the total spin operator $|\boldsymbol{S}|$ which is indicated for each line in Fig. 5.

In Tables I and II the fitted potential energy curves of the $X\ ^1\Sigma^+$ and $a\ ^3\Sigma^+$ states are given. The dispersion coefficients C_6 and C_8 are taken from Refs. [41,42]. With the present data sets we are also able to reproduce the experimental data with the same quality of the fit, by fixing these coefficients to the values from Ref. [40]. The reason for choosing the more recent values is that in this case the fitted C_{10} coefficient differs from the theoretical prediction by only −17%, whereas if the leading dispersion coefficients are fixed to the values from Ref. [40] the difference reaches +68% (the de-

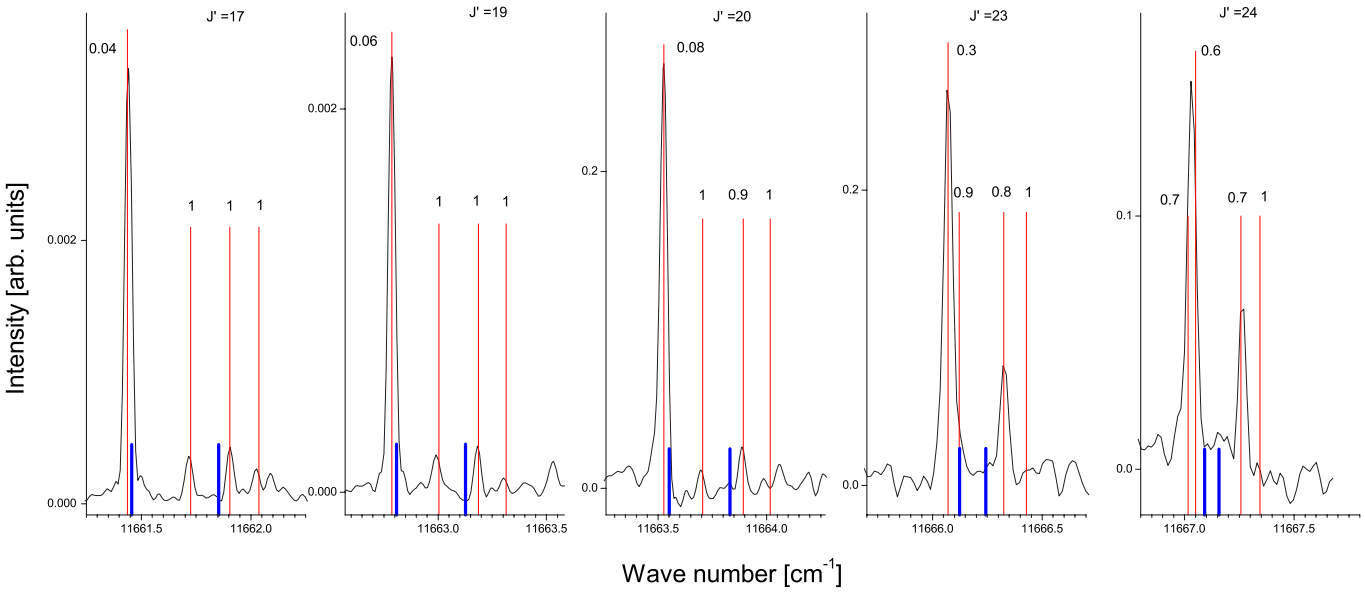

FIG. 5. (Color online) Observed transitions to $v_X''=49$ and $v_a''=10$ for different J' as indicated on the figure and excited by a Q-type transition. An extended portion of the spectrum for $J'=17$ for several v_a'' is shown in Fig. 3. For increasing J' the singlet and triplet lines approach each other, resulting in strong perturbations of the line structure and the intensity distribution within the HFS of the triplet line. Thick (blue) bars indicate the line positions as predicted by the Born-Oppenheimer potentials. Thin (red) bars indicate the prediction of the coupled channels calculation. The numbers close to these bars are the corresponding expectation values of the total spin operator $|\boldsymbol{S}|$. For convenience spectra are adjusted such that the largest peaks have similar intensities.

rived C_{10} amounts in this case to 2.39×10^{10} cm^{-1} Å^{10}). The selected set gives good consistency with the expected accuracy of most recent calculations of dispersion coefficients.

The potential curve at any point $R<R_o$ is defined by the natural cubic spline function through *all* points listed in Tables I and II. For $R\geqslant R_o$ the long-range parameters and expressions (1) and (2) should be used. For the convenience of the reader, we give in Tables I and II also T_e (energy of potential minimum), R_e (equilibrium distance), D_e (dissociation energy) and the dissociation energy D_0 with respect to the lowest rovibrational level ($v''=0$, $J''=0$ or $N''=0$). The model parameters for the potential are listed with all relevant figures necessary to reproduce the model with sufficient precision. The uncertainties of the dissociation energies have been estimated according to the data situation. The estimated uncertainty of the dissociation energy for the $a\ ^3\Sigma^+$ state is fairly large because of the limited data set, especially since no data are available yet for the lowest vibrational levels.

The derived $X\ ^1\Sigma^+$ state potential describes the experimental transition frequencies involving 2400 energy levels of the ground state with a standard deviation of 0.0057 cm^{-1} and a dimensionless standard deviation of $\bar{\sigma}=0.62$. The high standard deviation of the fit compared to the estimated error limits of 0.003 to 0.005 cm^{-1} from the typically applied experimental resolution of 0.03–0.05 cm^{-1} arises from the inclusion in the data analysis of a relatively large number of supplementary spectra (giving rise to about 26% of the identified transitions) recorded at lower resolution (0.1 cm^{-1}). The standard deviation for the experimental data with uncertainties less than 0.005 cm^{-1} (about 3600 transitions) amounts to 0.0030 cm^{-1} and $\bar{\sigma}$ for this case is 0.88. The increase of the dimensionless standard deviation is most likely due to overestimated error limits of the low resolution lines. The quality of the triplet state potential is assessed by comparing the experimental term energies with the calculated eigenvalues. The standard deviation amounts to 0.0044 cm^{-1} and the dimensionless standard deviation is 0.51.

In addition to the potential energy curves a set of Dunham coefficients was fitted to the data for the singlet ground state. These coefficients are given in Table V of the supplementary materials [32] and describe the experimental data for all rotational quantum numbers and a reduced set of v_X'', $0\leqslant v_X''\leqslant 45$.

V. APPLICATION TO COLD COLLISIONS

Cold collisions were studied for Li+Cs pairs through sympathetic cooling by Mudrich *et al.* [21] and through trap loss measurements by Schlöder *et al.* [20]. The latter work gives loss rates for processes where excited states are involved and thus cannot be related directly to cold collision calculations. These are now possible with the ground-state potentials reported in this paper. The former work derives the cross section for elastic scattering of unpolarized atomic pairs in the hyperfine ground states $f_{\mathrm{Li}}=1$ and $f_{\mathrm{Cs}}=3$ to be $8(4)\times10^{-12}$ cm^2 assuming Wigner's threshold behavior for s-wave scattering, i.e., the cross section is independent of collision energy. In this collision process the channels $f=2$, 3, and 4 of the total atomic angular momentum $\vec{f}=\vec{f}_{\mathrm{Li}}+\vec{f}_{\mathrm{Cs}}$ are involved. Using the potentials reported in this work the cross sections of these elastic channels were calculated for an energy range up to 100 μK. The values for $f=3$ and $f=2$ are at least an order of magnitude smaller than that of $f=4$, so only this channel should be taken into account for the com-

TABLE I. Pointwise representation of the potential energy curve for the $X\ ^1\Sigma^+$ state of LiCs. See also Table V of the supplementary materials [32]. The values of C_6 and C_8 are from Refs. [41,42].

R (Å)	U (cm^{-1})	R (Å)	U (cm^{-1})
2.110000	23121.37091	4.898338	2503.26403
2.193910	18288.09701	5.035379	2854.02395
2.277810	14589.99494	5.172421	3188.23112
2.361720	11737.62964	5.309462	3502.00098
2.445630	9497.25485	5.446503	3792.60234
2.529540	7805.39559	5.583500	4058.26131
2.613440	6434.86554	5.763111	4367.79625
2.697350	5258.36144	5.942722	4633.88339
2.781259	4228.82452	6.122333	4858.92343
2.865166	3334.95455	6.301944	5046.60206
2.949073	2568.92046	6.481556	5201.36003
3.032980	1922.48746	6.661167	5327.82056
3.116800	1387.62221	6.840778	5430.48784
3.253841	728.62698	7.020389	5513.45725
3.390883	302.73498	7.200000	5580.28406
3.527924	71.68736	7.550000	5675.34592
3.664966	0.03204	7.900000	5737.67458
3.802007	56.01497	8.250000	5778.85417
3.939048	211.90321	8.600000	5806.38135
4.076090	443.87130	8.950000	5825.08952
4.213131	731.70689	9.300000	5837.98033
4.350172	1058.39492	10.225000	5856.82445
4.487214	1409.72907	11.150000	5865.32302
4.624255	1773.86942	12.075000	5869.51458
4.761297	2141.05773	13.000000	5871.76955

$U_\infty = 5875.45504\ cm^{-1}$
$R_o = 11.5275$ Å
$C_6 = 1.47714 \times 10^7\ cm^{-1}$ Å^6 $A_{ex} = 3.81419 \times 10^4\ cm^{-1}$ Å$^{-\gamma}$
$C_8 = 4.33209 \times 10^8\ cm^{-1}$ Å^8 $\gamma = 5.0568$
$C_{10} = 1.21271 \times 10^{10}\ cm^{-1}$ Å^{10} $\beta = 2.2006$ Å^{-1}
$T_e^X = 0\ cm^{-1}$ $R_e^X = 3.6681$ Å
$D_e^X = 5875.455(100)\ cm^{-1}$ $D_0^X = 5783.408(100)\ cm^{-1}$

parison to the experimentally derived value which has 50% uncertainty. The value of this cross section varies only from 2.5 to 2.0×10^{-12} cm^2 from zero to 100 μK energy. Thus the threshold law is sufficiently well fulfilled. By weighting the cross section of $f=4$ with the statistical weight $9/(9+7+5)$ according to all existing channels we obtain a cross section of the unpolarized collision of 1.1×10^{-12} cm^2, which is about a factor of 8 smaller than that derived from the experiment, but within 2 times the given error. The potential for the singlet ground state is well determined by a large body of data (2397 levels), but the triplet ground state was only determined by 89 levels. Thus we believe that the difference between the two results indicates a need for more spectroscopic data, more precise cross section measurements, or a direct observation of Feshbach resonances. These can be incorporated in the fit of potential functions to obtain a full description of the spectroscopy and the cold collisions of Li+Cs atom pairs. The scattering length of the singlet ground state is well determined by the present study and is calculated to be $50(20)a_0$ (atomic unit $a_0 = 0.529 \times 10^{-10}$ m). In the case of the triplet state, however, large values with different signs were obtained when using potentials represented by spline coefficients as compared to piecewise analytic functions as used in some of our other work (see, e.g., [29]). Thus, such values of the scattering length of the triplet state are not yet reliable and calculations of Feshbach resonances would be of no value.

VI. CONCLUSION

In this work highly accurate potentials for the LiCs singlet and triplet ground states were derived from experimental

TABLE II. Pointwise representation of the potential energy curve for the $a\ ^3\Sigma^+$ state of LiCs. See also Table V of the supplementary materials [32]. The values of C_6 and C_8 are from Refs. [41,42].

R (Å)	U (cm^{-1})	R (Å)	U (cm^{-1})
3.020000	10529.73474	7.673846	5783.12762
3.384521	8133.49216	8.093333	5805.67410
3.749042	6806.18429	8.512821	5822.85769
4.113562	6133.96772	8.932308	5835.76854
4.478083	5768.93998	9.597282	5849.85069
4.769700	5630.11787	10.190769	5857.88706
5.318264	5567.01710	11.000000	5864.74252
5.866825	5613.25953	12.000000	5869.36430
6.415385	5676.25455	13.000000	5871.79045
6.834872	5718.42584	14.000000	5873.16557
7.254359	5754.16017		
U_∞=5875.45504 cm^{-1}			
R_o=11.5183 Å			
C_6=1.47714×10^7 cm^{-1} $Å^6$		A_{ex}=3.81419×10^4 cm^{-1} $Å^{-\gamma}$	
C_8=4.33209×10^8 cm^{-1} $Å^8$		γ=5.0568	
C_{10}=1.21271×10^{10} cm^{-1} $Å^{10}$		β=2.2006 $Å^{-1}$	
T_e^a=5566.0898 cm^{-1}		R_e^a=5.2472 Å	
D_e^a=309(10) cm^{-1}		D_0^a=287(10) cm^{-1}	

data. They also provide precise information on dissociation energies and equilibrium internuclear distances and enable modeling of cold collisions.

Previously, the most accurate potentials were based on *ab initio* calculations [27], the quality of which we estimate by comparing two quantities, namely the dissociation energy D_e and the equilibrium internuclear separation R_e because a graphical comparison is generally too rough. For the $X\ ^1\Sigma^+$ state we find D_e=5875.455 cm^{-1} and R_e=3.6681 Å with the corresponding *ab initio* results being 5996 cm^{-1} and 3.615 Å, respectively [27]. For the $a\ ^3\Sigma^+$ state the present work reveals D_e=309 cm^{-1} and R_e=5.2472 Å, while the corresponding *ab initio* calculations give, respectively, 307 cm^{-1} and 5.229 Å.

The difference in the dissociation energies in the case of the singlet state could correspond to at least one vibrational level more than the total number of levels accommodated in the derived potential (55 for J=0), but for the triplet state the agreement is surprisingly good. The good agreement may be explained by the fact that we used the *ab initio* potential as a starting point for our fits and due to the lack of low vibrational levels in the data set its shape around the minimum has not been changed significantly by the fitting program. The amplitude of the exchange interaction which can be estimated from the difference of the theoretical asymptotic singlet and triplet potentials comes close (30%) to the value from the fit.

In their experimental work on the $X\ ^1\Sigma^+$ state Kanes *et al.* [24] determined, with the aid of some theoretical data, a dissociation energy of 0.72 eV (~5800 cm^{-1}). Within its 10% uncertainty this number is in good agreement with our determination of the dissociation energy.

The present potentials can be applied to model cold collisions. The calculated cross section for elastic scattering agrees with the one measured in Ref. [21] within 2 times the experimental uncertainty. A more accurate comparison requires a more precise cross section measurement and more spectroscopic data. Based on the present potential curves a scattering length of 50(20)a_0 is calculated for the singlet ground state whereas for the triplet ground state a meaningful number cannot be derived. To make such calculations reliable, and to accurately predict Feshbach resonances, more spectroscopic data for the low vibrational levels of the $a\ ^3\Sigma^+$ state and of near asymptotic levels of both ground states are needed.

In addition to collecting data by exciting to high-lying levels of the $B\ ^1\Pi$ state we searched for, but did not find, other excitation channels that lead to combined fluorescence to both ground states, especially to asymptotic levels. For improving predictions of appropriate excitations we have started experiments to obtain precise data for various excited states. The analysis of the states $B\ ^1\Pi$ and $D\ ^1\Pi$ is almost complete and will be presented in a forthcoming paper [35].

ACKNOWLEDGMENTS

This work was supported by the Deutsche Forschungsgemeinschaft in the frame of the Sonderforschungsbereich 407 and by the European Commission in the frame of the Cold Molecule Research Training Network under Contract No. HPRN-CT-2002-00290. One of the authors (A.P.) acknowledges partial support from the Bulgarian National Science Fund Grants No. MUF 1506/05 and No. VUF 202/06.

[1] S. D. Kraft, P. Staanum, J. Lange, L. Vogel, R. Wester, and M. Weidemüller, J. Phys. B **39**, S993 (2006).
[2] M. W. Mancini, G. D. Telles, A. R. L. Caires, V. S. Bagnato, and L. G. Marcassa, Phys. Rev. Lett. **92**, 133203 (2004).
[3] D. Wang, J. Qi, M. F. Stone, O. Nikolayeva, H. Wang, B. Hattaway, S. D. Gensemer, P. L. Gould, E. E. Eyler, and W. C. Stwalley, Phys. Rev. Lett. **93**, 243005 (2004).
[4] C. Haimberger, J. Kleinert, M. Bhattacharya, and N. P. Bigelow, Phys. Rev. A **70**, 021402(R) (2004).
[5] A. J. Kerman, J. M. Sage, S. Sainis, T. Bergeman, and D. DeMille, Phys. Rev. Lett. **92**, 153001 (2004).
[6] M. Aymar and O. Dulieu, J. Chem. Phys. **122**, 204302 (2005).
[7] G. Igel-Mann, U. Wedig, P. Fuentealba, and H. Stoll, J. Chem. Phys. **84**, 5007 (1986).
[8] R. Krems, Int. Rev. Phys. Chem. **24**, 99 (2005).
[9] R. V. Krems, Phys. Rev. Lett. **96**, 123202 (2006).
[10] N. Balakrishnan and A. Dalgarno, Chem. Phys. Lett. **341**, 652 (2001).
[11] E. Bodo, F. Gianturco, and A. Dalgarno, J. Chem. Phys. **116**, 9222 (2002).
[12] D. DeMille, Phys. Rev. Lett. **88**, 067901 (2002).
[13] D. Wang, E. E. Eyler, P. L. Gould, and W. C. Stwalley, Phys. Rev. A **72**, 032502 (2005).
[14] J. M. Sage, S. Sainis, T. Bergeman, and D. DeMille, Phys. Rev. Lett. **94**, 203001 (2005).
[15] B. DeMarco and D. S. Jin, Science **285**, 1703 (1999).
[16] G. Modugno, G. Ferrari, G. Roati, R. J. Brecha, A. Simoni, and M. Inguscio, Science **294**, 1320 (2001).
[17] A. G. Truscott, K. E. Strecker, W. I. McAlexander, G. B. Partridge, and R. G. Hulet, Science **291**, 2570 (2001).
[18] K. Mølmer, Phys. Rev. Lett. **80**, 1804 (1998).
[19] H. Heiselberg, C. J. Pethick, H. Smith, and L. Viverit, Phys. Rev. Lett. **85**, 2418 (2000).
[20] U. Schlöder, H. Engler, U. Schünemann, R. Grimm, and M. Weidemüller, Eur. Phys. J. D **7**, 331 (1999).
[21] M. Mudrich, S. Kraft, K. Singer, R. Grimm, A. Mosk, and M. Weidemüller, Phys. Rev. Lett. **88**, 253001 (2002).
[22] R. Gonzalez-Ferez, M. Mayle, and P. Smelcher, Chem. Phys. **329**, 203 (2006).
[23] J. M. Walter and S. Barratt, Proc. R. Soc. London, Ser. A **119**, 257 (1928).
[24] H. Kanes, H. Pauly, and E. Vietzke, Z. Naturforsch. A **26A**, 689 (1971).
[25] C. Vadla, C.-J. Lorenzen, and K. Niemax, Phys. Rev. Lett. **51**, 988 (1983).
[26] M. Mudrich, O. Bünermann, F. Stienkemeier, O. Dulieu, and M. Weidemüller, Eur. Phys. J. D **31**, 291 (2004).
[27] M. Korek, A. R. Allouche, K. Fakhreddine, and A. Chaalan, Can. J. Phys. **78**, 977 (2000).
[28] A. Pashov, O. Docenko, M. Tamanis, R. Ferber, H. Knöckel, and E. Tiemann, Phys. Rev. A **72**, 062505 (2005).
[29] O. Docenko, M. Tamanis, J. Zaharova, R. Ferber, A. Pashov, H. Knöckel, and E. Tiemann, J. Phys. B **39**, S929 (2006).
[30] O. Docenko, M. Tamanis, R. Ferber, A. Pashov, H. Knöckel, and E. Tiemann, Eur. Phys. J. D **31**, 205 (2004).
[31] V. Bednarska, I. Jackowska, W. Jastrzębski, and P. Kowalczyk, Meas. Sci. Technol. **7**, 1291 (1996).
[32] See EPAPS Document No. E-PLRAAN-75-040704 for supplementary tables containing lists of fluorescence progressions to the $X\ ^1\Sigma^+$ and $a\ ^3\Sigma^+$ states, excitation transitions in the $D\ ^1\Pi \leftarrow X\ ^1\Sigma^+$ and $B\ ^1\Pi \leftarrow X\ ^1\Sigma^+$ bands as well as the potential energy curves given in Tables I and II of the paper and a set of Dunham coefficients for the $X\ ^1\Sigma^+$ state . For more information on EPAPS, see http://www.aip.org/pubservs/epaps.html.
[33] A. Pashov, W. Jastrzębski, and P. Kowalczyk, Comput. Phys. Commun. **128**, 622 (2000).
[34] G. Audi, A. Wapstra, and C. Thibault, Nucl. Phys. A **729**, 337 (2003).
[35] A. Pashov, A. Stein, P. Staanum, H. Knöckel, and E. Tiemann (unpublished).
[36] S. Kasahara, T. Ebi, M. Tanimura, H. I. K. Matsubara, M. Baba, and H. Katô, J. Chem. Phys. **105**, 1341 (1996).
[37] E. Arimondo, M. Inguscio, and P. Violino, Rev. Mod. Phys. **49**, 31 (1977).
[38] B. M. Smirnov and M. I. Chibisov, Zh. Eksp. Teor. Fiz. **48**, 939 (1965).
[39] O. Allard, A. Pashov, H. Knöckel, and E. Tiemann, Phys. Rev. A **66**, 042503 (2002).
[40] M. Marinescu and H. R. Sadeghpour, Phys. Rev. A **59**, 390 (1999).
[41] A. Derevianko, J. F. Babb, and A. Dalgarno, Phys. Rev. A **63**, 052704 (2001).
[42] S. G. Porsev and A. Derevianko, J. Chem. Phys. **119**, 844 (2003).
[43] A. A. Radzig and P. M. Smirnov, *Reference Data on Atoms, Molecules and Ions* (Springer, Berlin, 1985).
[44] C. A. Stan and W. Ketterle, Rev. Sci. Instrum. **76**, 063113 (2005).
[45] Note that the CF flange on the side container [30] is here closed using a nickel gasket; traditional copper gaskets are corroded by Li [44].
[46] Here N is the rotational quantum number for a Hund's case (b) state and the total angular momentum $\boldsymbol{J}$ is the sum of $\boldsymbol{N}$ and the total electron spin $\boldsymbol{S}$.